

The Parker Scenario for Coronal Heating as an MHD Turbulence Problem

A.F. Rappazzo¹, M. Velli^{1,2}, and G. Einaudi³

Abstract. The Parker or field line tangling model of coronal heating is investigated through long-time high-resolution simulations of the dynamics of a coronal loop in cartesian geometry within the framework of reduced magnetohydrodynamics (RMHD). Slow photospheric motions induce a Poynting flux which saturates by driving an anisotropic turbulent cascade dominated by magnetic energy and characterized by current sheets elongated along the axial magnetic field. Increasing the value of the axial magnetic field different regimes of MHD turbulence develop with a bearing on coronal heating rates. In physical space magnetic field lines at the scale of convection cells appear only slightly bended in agreement with observations of large loops of current (E)UV and X-ray imagers.

1. Introduction

Coronal heating is one of the outstanding problems in solar physics. Although the correlation of coronal activity with the intensity of photospheric magnetic fields seems beyond doubt, and there is large agreement that photospheric motions are the source of the energy flux that sustains an active region ($\sim 10^7 \text{ erg cm}^{-2} \text{ s}^{-1}$), the debate currently focuses on the physical mechanisms responsible for the transport, storage and dissipation (i.e. conversion to heat and/or particle acceleration) of this energy from the photosphere to the corona.

A promising model is that proposed by Parker (1972, 1988), who suggested that coronal heating could be the necessary outcome of an energy flux associated with the tangling of coronal field lines by photospheric motions.

Over the years numerous analytical and numerical investigations (Parker 1972; Sturrock and Uchida 1981; van Ballegoijen 1986; Mikic et al. 1989; Parker 1988; Berger 1991; Heyvaerts & Priest 1992; Gomez & Ferro-Fontan 1992; Longcope & Sudan 1994; Hendrix & Van Hoven 1996; Einaudi et al. 1996; Georgoulis et al. 1998; Dmitruk et al. 1998; Dmitruk & Gómez 1999; Einaudi & Velli 1999) have been carried out, discussing in some details different aspects of the problem.

In all 3D cartesian simulations a complex coronal magnetic field results from the photospheric footpoints motions, and though the field does not, strictly speaking, evolve through a sequence of static force-free equilibrium states (the original Parker hypothesis), magnetic energy nonetheless tends to dominate kinetic energy, and current sheets elongated along the axial direction characterize

¹Jet Propulsion Laboratory, California Institute of Technology, Pasadena, CA, 91109 USA

²Dipartimento di Astronomia e Scienza dello Spazio, Università di Firenze, 50125 Florence, Italy

³Dipartimento di Fisica “E. Fermi”, Università di Pisa, 56127 Pisa, Italy

the system. The results from these studies agreed qualitatively among themselves, in that all simulations display the development of field aligned current sheets. However, estimates of the dissipated power and its scaling characteristics differed largely, depending on the way in which extrapolations from low to large values of the plasma conductivity of the properties such as inertial range power law indices were carried out. Furthermore, the physical mechanism responsible for current sheets formation was not conclusively determined.

More recently a first attempt to simulate full 3D sections of the solar corona with a realistic geometry has been performed by Gudiksen & Nordlund (2005). At the moment the very low resolution attainable with this kind of simulations does not allow the development of turbulence. The transfer of energy from the scale of convection cells $\sim 1000 \text{ km}$ toward smaller scales is in fact inhibited, because the smaller scales are not resolved (their linear resolution is in fact $\sim 500 \text{ km}$).

While in the future these global simulations will be able to reach the necessary high resolutions, to investigate the nonlinear dynamics of the Parker scenario at relatively high Reynolds numbers, we have recently performed high-resolution long-time simulation of the aforementioned cartesian model (Rappazzo et al. (2007)).

In the next sections we describe the coronal loop model, the simulations we have carried out, and give simple scaling arguments to understand the energy spectral slopes.

2. Physical model

A coronal loop is a closed magnetic structure threaded by a strong axial field, with the footpoints rooted in the photosphere. This makes it a strongly anisotropic system, as measured by the relative magnitude of the Alfvén velocity associated with the axial magnetic field $v_A \sim 2000 \text{ km s}^{-1}$ compared to the typical photospheric velocity $u_{ph} \sim 1 \text{ km s}^{-1}$. This means that the relative amplitude of the Alfvén waves that are launched into the corona is very small and, as an efficient energy cascade takes place (Rappazzo et al. 2007), the relative amplitude of the fields which develop in the orthogonal planes remains small compared to the dominant axial magnetic field.

We study the loop dynamics in a simplified cartesian geometry, neglecting any curvature effect, as a “straightened out” box, with an orthogonal square cross section of size ℓ (along which the x-y directions lie), and an axial length L (along the z direction) embedded in an axial homogeneous uniform magnetic field $\mathbf{B}_0 = B_0 \mathbf{e}_z$. This simplified geometry allows us to perform simulations with both high numerical resolution and long-time duration.

The dynamics of a plasma embedded in a strong axial magnetic field are well described by the equations of reduced MHD (Kadomtsev & Pogutse 1974; Strauss 1976; Montgomery 1982). In this limit the velocity and magnetic fields have only perpendicular components, linked to the velocity and magnetic potentials φ and ψ by

$$\mathbf{u}_\perp = \nabla \times (\varphi \mathbf{e}_z), \quad \mathbf{b}_\perp = \nabla \times (\psi \mathbf{e}_z). \quad (1)$$

Although numerically we advance the equations for the potentials in order to analyze the linear and nonlinear properties of the system it is convenient to write the equivalent equations using the Elsässer variables $\mathbf{z}^\pm = \mathbf{u}_\perp \pm \mathbf{b}_\perp$. The more symmetric equations, which explicit the underlying physical processes at work, are given in dimensionless form by:

$$\frac{\partial \mathbf{z}^+}{\partial t} = -(\mathbf{z}^- \cdot \nabla_\perp) \mathbf{z}^+ + \frac{v_A}{u_{ph}} \frac{\partial \mathbf{z}^+}{\partial z} + \frac{1}{\mathcal{R}} \nabla_\perp^2 \mathbf{z}^+ - \nabla_\perp P \quad (2)$$

$$\frac{\partial \mathbf{z}^-}{\partial t} = -(\mathbf{z}^+ \cdot \nabla_\perp) \mathbf{z}^- - \frac{v_A}{u_{ph}} \frac{\partial \mathbf{z}^-}{\partial z} + \frac{1}{\mathcal{R}} \nabla_\perp^2 \mathbf{z}^- - \nabla_\perp P \quad (3)$$

$$\nabla_\perp \cdot \mathbf{z}^\pm = 0 \quad (4)$$

where $P = p + \mathbf{b}_\perp^2/2$ is the total pressure, and is linked to the nonlinear terms by incompressibility (4):

$$\nabla_\perp^2 P = - \sum_{i,j=1}^2 \left(\partial_i z_j^- \right) \left(\partial_j z_i^+ \right). \quad (5)$$

The gradient operator has only components in the x - y plane perpendicular to the axial direction z , and the dynamics in the orthogonal planes is coupled to the axial direction through the linear terms $\propto \partial_z$.

We use a computational box with an aspect ratio of 10, which then spans

$$0 \leq x, y \leq 1, \quad 0 \leq z \leq 10. \quad (6)$$

The linear terms $\propto \partial_z$ are multiplied by the dimensionless parameter v_A/u_{ph} , the ratio between the Alfvén velocity associated with the axial magnetic field $v_A = B_0/\sqrt{4\pi\rho_0}$, and the photospheric velocity u_{ph} .

Boundary conditions for our numerical simulations are specified imposing the velocity potential $\varphi(x, y)$ in the bottom ($z = 0$) and top ($z = L$) planes:

$$\varphi(x, y) = \frac{1}{\sqrt{\sum_{m,n} \alpha_{mn}^2}} \sum_{k,l} \frac{\alpha_{kl}}{2\pi\sqrt{k^2 + l^2}} \sin [2\pi (kx + ly) + 2\pi\xi_{kl}]. \quad (7)$$

These result from the linear combination of large-scale eddies with random amplitudes α_{kl} and phases ξ_{kl} (whose values are included between 0 and 1). We excite all the twelve independent modes whose wave-numbers are included in the range $3 \leq (k^2 + l^2)^{1/2} \leq 4$, and then normalize the result so that the velocity rms is $\sim 1 \text{ km s}^{-1}$.

In terms of the Elsässer variables \mathbf{z}^\pm , to impose a velocity pattern (\mathbf{u}_\perp^*) at the boundary surfaces means to impose the constraint $\mathbf{z}^+ + \mathbf{z}^- = 2\mathbf{u}_\perp^*$, and as in terms of characteristics (which in this case are simply \mathbf{z}^\pm themselves) we can specify only the incoming wave (while the outgoing wave is determined by the dynamics inside the computational box), at the top ($z = L$) and bottom ($z = 0$) planes the following “reflection” takes place:

$$\mathbf{z}^- = -\mathbf{z}^+ + 2\mathbf{u}_\perp^0 \quad \text{at } z = 0 \quad (8)$$

$$\mathbf{z}^+ = -\mathbf{z}^- + 2\mathbf{u}_\perp^L \quad \text{at } z = L \quad (9)$$

where \mathbf{u}_\perp^0 and \mathbf{u}_\perp^L are the forcing functions in the respective boundary surfaces.

At time $t = 0$ no perturbation is imposed inside the computational box, i.e. $\mathbf{b}_\perp = \mathbf{u}_\perp = 0$, and only the axial magnetic field B_0 is present: the subsequent dynamics are then the effect of the photospheric forcing on the system.

The linear terms ($\propto \partial_z$) in equations (2)-(3) give rise to two distinct wave equations for the \mathbf{z}^\pm fields, which describe Alfvén waves propagating along the axial direction z . This wave propagation, which is present during both the linear and nonlinear stages, is responsible for the transport of energy at the large perpendicular scales from the boundaries (photosphere) into the loop. The nonlinear terms ($\mathbf{z}^\mp \cdot \nabla_\perp$) \mathbf{z}^\pm are then responsible for the transport of this energy from the large scales toward the small scales, where energy is finally dissipated, i.e. converted to heat and/or particle acceleration.

An important feature of the nonlinear terms in equations (2)-(4) is the absence of self-coupling, i.e. they only couple counterpropagating waves, and if one of the two fields \mathbf{z}^\pm were zero, there would be no nonlinear dynamics at all. This is at the basis of the so-called Alfvén effect (Iroshnikov 1964; Kraichnan 1965), that ultimately renders the nonlinear timescales longer and slows down the dynamics.

From this analysis it is clear that three different timescales are present: τ_A , τ_{ph} and τ_{nl} . $\tau_A = L/v_A$ is the crossing time of the Alfvén waves along the axial direction z , i.e. the time it takes for an Alfvén wave to cover the loop length L . $\tau_{ph} \sim 5 m$ is the characteristic time associated with photospheric motions, while τ_{nl} is the nonlinear timescale.

For a typical coronal loop $\tau_A \ll \tau_{ph}$, and for this reason we consider a forcing which is constant in time, i.e. for which formally $\tau_{ph} = \infty$.

In the RMHD ordering the nonlinear timescale τ_{nl} is bigger than the Alfvén crossing time τ_A . This ordering is confirmed and maintained throughout our numerical simulations.

The length of a coronal section is taken as the unitary length, but as we excite all the wavenumbers between 3 and 4, and the typical convection cell scale is $\sim 1000 km$, this implies that each side of our section is roughly $4000 km$ long. Our grid for the cross-sections has 512×512 grid points, corresponding to $\sim 128^2$ points per convective cell, and hence a linear resolution of $\sim 8 km$.

Between the top and bottom plate a uniform magnetic field $\mathbf{B} = B_0 \mathbf{e}_z$ is present. The subsequent evolution is due to the shuffling of the footpoints of the magnetic field lines by the photospheric forcing.

In this section we present the results of a simulation performed with a numerical grid with $512 \times 512 \times 200$ points, Reynolds number $\mathcal{R} = 800$, and the Alfvén velocity $v_A = 200 km s^{-1}$ corresponding to a ratio $v_A/u_{ph} = 200$. The total duration is roughly 500 axial Alfvén crossing times ($\tau_A = L/v_A$).

Plots of the total magnetic and kinetic energies

$$E_M = \frac{1}{2} \int dV \mathbf{b}_\perp^2, \quad E_K = \frac{1}{2} \int dV \mathbf{u}_\perp^2, \quad (10)$$

and of the total magnetic (J) and kinetic (Ω) dissipation rates

$$J = \frac{1}{\mathcal{R}} \int dV \mathbf{j}^2 \quad \Omega = \frac{1}{\mathcal{R}} \int dV \boldsymbol{\omega}^2 \quad (11)$$

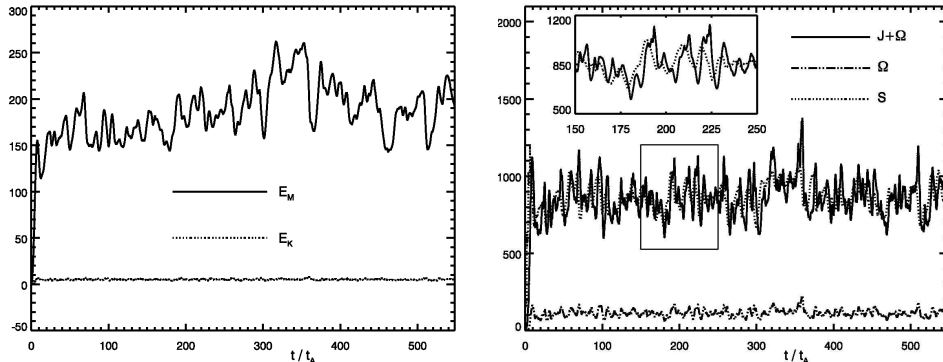


Figure 1.: High-resolution simulation with $v_A/u_{ph} = 200$, $512 \times 512 \times 200$ grid points and $\mathcal{R} = 800$. *Left*: Magnetic (E_M) and kinetic (E_K) energies as a function of time ($\tau_A = L/v_A$ is the axial Alfvénic crossing time). *Right*: The integrated Poynting flux S dynamically balances the total dissipation D . Inset shows a magnification of total dissipation and S for $180 \leq t/\tau_A \leq 280$.

along with the incoming energy rate (Poynting flux) S , are shown in Figure 1. At the beginning the system has a linear behavior, characterized by a time linear growth rate for the magnetic energy, the Poynting flux and the electric current, until time $t \sim 6\tau_A$, when nonlinearity sets in. The magnetic energy is bigger than the kinetic energy, this is the natural result of the field line bending due to the photospheric motions both in the linear and nonlinear stages. More formally this is a consequence of the fact that, while on the perpendicular magnetic field no boundary condition is imposed, the velocity field must approach the imposed boundary values at the photosphere both during the linear and nonlinear stages.

After this time, in the fully nonlinear stage, a *statistically steady state* is reached, in which the Poynting flux, i.e. the energy that is entering the system for unitary time, balances on time average the total dissipation rate ($J + \Omega$). As a result there is no average accumulation of energy in the box, beyond what has been accumulated during the linear stage, and a detailed examination of the dissipation time series (see inset in Figure 1) shows that the Poynting flux and total dissipations are decorrelated around dissipation peaks.

Correspondingly, in Fourier space, we have shown (see Rappazzo et al. 2007) that the spectral index for total energy fits well the -2 value. We have also shown that this spectral index strongly depends on the ratio v_A/u_{ph} , i.e. on the relative strength of the axial magnetic field. At lower values correspond flatter spectra, with an index close to $-5/3$ (Kolmogorov), while to higher values of the magnetic field the spectra steepens up to $\sim -5/2$ for $v_A/u_{ph} \sim 1000$.

Figure 2 shows a snapshot, at time $t \sim 18\tau_A$, of current sheets and field lines of total magnetic field.

3. Conclusion and discussion

Recently a lot of progress has been made in the understanding of MHD turbulence for a system embedded in a strong magnetic field, both in the con-

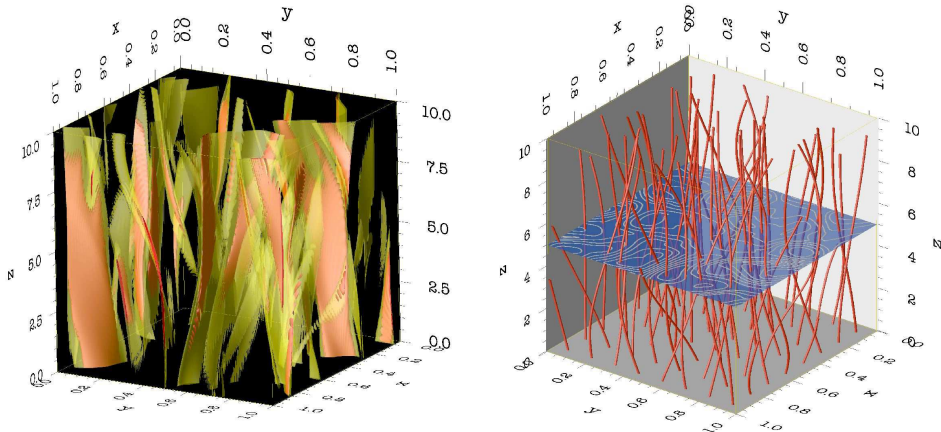


Figure 2.: *Left*: Snapshot of current sheets elongated along the axial direction. *Right*: Magnetic field lines are not much entangled because an efficient energy cascade takes place. Mid-plane shows field-lines of the orthogonal magnetic field. *The box has been rescaled for an improved viewing. The box has an aspect ratio of 10, to restore the original aspect ratio the box should be stretched 10 times along the axial direction z .*

dition of so-called weak (Ng & Bhattacharjee 1997; Goldreich & Sridhar 1997; Galtier et al. 2000) and strong turbulence (Goldreich & Sridhar 1995, 1997; Cho & Vishniac 2000; Biskamp & Müller 2000; Müller et al. 2003; Müller & Grappin 2005). In particular it has been developed (Boldyrev 2005, 2006; Mason et al. 2006) a cascade model that self-consistently accounts for current sheets formation.

The presence of dynamical current sheets elongated along the direction of the strong axial magnetic field, that are continuously formed and dissipated, is most properly accounted for in the framework of MHD turbulence. In fact, two important characteristic of MHD turbulence are that the cascade takes place mainly in the plane orthogonal to the local mean magnetic field (Shebalin et al. 1983), where small scales form, and that the small scales are not uniformly distributed in this plane. Rather they are organized in current-vortex sheets aligned along the direction of the local main field, and *constitute the dissipative structures of MHD turbulence* (e.g. Biskamp & Müller (2000), Biskamp (2003) and references therein). When the system is threaded by a strong axial magnetic field, as in our case, the cascade takes place mainly in the orthogonal planes, and the current sheets are elongated along the axial direction (Figure 2).

The fact that at the large orthogonal scales the Alfvén crossing time τ_A is the fastest timescale, and in particular it is smaller than the nonlinear timescale τ_{nl} (which can be identified with the energy transfer time at the driving scale), implies that the Alfvén waves that continuously propagate and reflect from the boundaries toward the interior are basically equivalent to an anisotropic magnetic forcing function that stirs the fluid, whose orthogonal length is that of the convective cells (~ 1000 km) and whose axial length is given by the loop length L .

The spectra that we have found can be easily derived by order of magnitude considerations. Dimensionally, and integrating over the whole box, the energy cascade rate may be written as

$$\epsilon \sim \ell_{\perp}^2 L \rho \frac{\delta z_{\lambda}^2}{T_{\lambda}}, \quad (12)$$

where δz_{λ} is the rms value of the Elsässer fields $\mathbf{z}^{\pm} = \mathbf{u}_{\perp} \pm \mathbf{b}_{\perp}$ at the perpendicular scale λ . Given the symmetry of the system it is expected and confirmed numerically that cross helicity is zero, hence $\delta z_{\lambda}^{+} \sim \delta z_{\lambda}^{-} \sim \delta z_{\lambda}$. ρ is the average density and T_{λ} is the energy transfer time at the scale λ , which is greater than the eddy turnover time $\tau_{\lambda} \sim \lambda/\delta z_{\lambda}$ because of the Alfvén effect (Iroshnikov 1964; Kraichnan 1965).

In the classical IK case $T_{\lambda} \sim \tau_{\lambda} (\tau_{\lambda}/\tau_A)$. More generally, however, as the Alfvén speed is increased nonlinear interactions become weaker. Simply from dimensional considerations as the ratio τ_{λ}/τ_A is dimensionless and smaller than 1, we can suppose that the energy transfer time scales as

$$T_{\lambda} \sim \tau_{\lambda} \left(\frac{\tau_{\lambda}}{\tau_A} \right)^{\alpha-1}, \quad \text{with} \quad \alpha \geq 1, \quad (13)$$

where α is the scaling index (note that $\alpha = 1$ corresponds to standard hydrodynamic turbulence).

Substituting (13) in (12) we can compute the energy transfer rate. As this is supposed to be constant along the inertial range, considering the injection scale $\lambda \sim \ell_{\perp}$, the energy transfer rate (12) becomes

$$\epsilon \sim \ell_{\perp}^2 L \cdot \rho \frac{\delta z_{\ell_{\perp}}^2}{T_{\ell_{\perp}}} \sim \frac{\rho \ell_{\perp}^2 L^{\alpha}}{\ell_{\perp}^{\alpha} v_A^{\alpha-1}} \delta z_{\ell_{\perp}}^{\alpha+2}. \quad (14)$$

On the other hand the energy injection rate is given by the Poynting flux integrated across the photospheric boundaries: $\epsilon_{in} = \rho v_A \int da \mathbf{u}_{ph} \cdot \mathbf{b}_{\perp}$. Considering that this integral is dominated by energy at the large scales, due to the characteristics of the forcing function, we can approximate it with

$$\epsilon_{in} \sim \rho \ell_{\perp}^2 v_A u_{ph} \delta z_{\ell_{\perp}}, \quad (15)$$

where the large scale component of the magnetic field can be replaced with $\delta z_{\ell_{\perp}}$ because the system is magnetically dominated.

The last two equations show that the system is self-organized because both ϵ and ϵ_{in} depend on $\delta z_{\ell_{\perp}}$, the rms values of the fields \mathbf{z}^{\pm} at the scale ℓ_{\perp} : the internal dynamics depends on the injection of energy and the injection of energy itself depends on the internal dynamics via the boundary forcing.

In a stationary cascade the injection rate (15) is equal to the transport rate (14). Equating the two determines $\delta z_{\ell_{\perp}}$, that substituted in (14) or (15) yields to the energy flux

$$\epsilon^* \sim \ell_{\perp}^2 \rho v_A u_{ph}^2 \left(\frac{\ell_{\perp} v_A}{L u_{ph}} \right)^{\frac{\alpha}{\alpha+1}}, \quad (16)$$

where $v_A = B_0/\sqrt{4\pi\rho}$. This is also the dissipation rate, and hence the *coronal heating scaling*. A dimensional analysis of eqs. (2)-(4) reveals (see Rappazzo et al. 2007) that the only free parameter is $f = \ell_\perp v_A/Lu_{ph}$, so that the scaling index α (13), upon which the strength of the stationary turbulent regime depends, must be a function of f itself, and we have determined its value computationally (Rappazzo et al. 2007).

Dividing eq. (16) by the surface ℓ_\perp^2 we obtain the energy flux per unit area $F = \epsilon^*/\ell_\perp^2$. Taking for example a coronal loop 40,000 km long, with a number density of 10^{10} cm^{-3} , $v_A = 2,000 \text{ km s}^{-1}$ and $u_{ph} = 1 \text{ km s}^{-1}$, which models an active region loop, we obtain $F \sim 5 \cdot 10^6 \text{ erg cm}^{-2} \text{ s}^{-1}$. On the other hand, for a coronal loop typical of a quiet Sun region, with a length of 100,000 km, a number density of 10^{10} cm^{-3} , $v_A = 500 \text{ km s}^{-1}$ and $u_{ph} = 1 \text{ km s}^{-1}$, we obtain $F \sim 7 \cdot 10^4 \text{ erg cm}^{-2} \text{ s}^{-1}$.

In summary, the Parker scenario for coronal heating may be considered as a MHD turbulence problem, self-consistently accounting for current sheets formation. The derived coronal heating rates scale with coronal loop and photospheric driving parameters, and there is not a single universal scaling law.

Acknowledgments. A.F.R. is supported by the NASA Postdoctoral Program, M.V. is supported by NASA LWS TR&T and SR&T. A.F.R. and M.V. thank the IPAM program ‘‘Grand Challenge Problems in Computational Astrophysics’’ at UCLA.

References

- Berger, M. A. 1991, A&A, 252, 369
 Biskamp, D. 2003, Magnetohydrodynamic Turbulence (Cambridge: Cambridge University Press)
 Biskamp, D. & Müller, W.-C. 2000, Phys. Plasmas, 7, 4889
 Boldyrev, S. 2005, ApJ, 626, L37
 Boldyrev, S. 2006, Phys. Rev. Lett., 96, 115002
 Cho, J. & Vishniac, E. T. 2000, ApJ, 539, 273
 Dmitruk, P., Gómez, D. O. & DeLuca, D. D. 1998, ApJ, 505, 974
 Dmitruk, P. & Gómez, D. O. 1999, ApJ, 527, L63
 Dmitruk, P., Gómez, D. O. & Matthaeus, W. H. 2003, Phys. Plasmas, 10, 3584
 Einaudi, G., Velli, M., Politano, H. & Pouquet, A. 1996, ApJ, 457, L113
 Einaudi, G. & Velli, M. 1999, Phys. Plasmas, 6, 4146
 Galtier, S., Nazarenko, S. V., Newell, A. C. & Pouquet, A. 2000, J. Plasma Phys., 63, 447
 Georgoulis, M. K., Velli, M. & Einaudi, G., 1998, ApJ, 497, 957
 Goldreich, P. & Sridhar, S. 1995, ApJ, 438, 763
 Goldreich, P. & Sridhar, S. 1997, ApJ, 485, 680
 Gomez, D.O. and Ferro-Fontan, C.F. 1992 ApJ, 394, 662
 Gudiksen, B. V. & Nordlund, Å. 2005, ApJ, 618, 1020
 Hendrix, D. L. & Van Hoven, G. 1996, ApJ, 467, 887
 Heyvaerts, J. and Priest, E.R. 1992, ApJ, 390, 297
 Iroshnikov, P. S. 1964, Sov. Astron., 7, 566
 Kadomtsev, B. B. & Pogutse, O. P. 1974, Sov. J. Plasma Phys., 1, 389
 Kraichnan, R. H. 1965, Phys. Fluids, 8, 1385
 Longcope, D. W. & Sudan, R. N. 1994, ApJ, 437, 491
 Mason, J., Cattaneo, F. & Boldyrev, S. 2006, Phys. Rev. Lett., 97, 255002

- Müller, W. C., Biskamp, D. & Grappin, R. 2003, Phys. Rev. E, 67, 066302
Müller, W. C. & Grappin, R. 2005, Phys. Rev. Lett., 95, 114502
Mikic, Z., Schnack, D. D. & Van Hoven, G. 1989, ApJ, 338, 1148
Montgomery, D. 1982, Phys. Scripta, T2/1, 83
Ng, C. S. & Bhattacharjee, A. 1997, Phys. Plasmas, 4, 605
Parker, E. N. 1972, ApJ, 174, 499
Parker, E. N. 1988, ApJ, 330, 474
Rappazzo, A. F., Velli, M., Einaudi, G. & Dahlburg, R. B. 2007, ApJ, 657, L47
Shebalin, J. V., Matthaeus, W. H. & Montgomery, D. 1983, J. Plasma Phys., 29, 525
Sridhar, S. & Goldreich, P. 1994, ApJ, 432, 612
Strauss, H. R. 1976, Phys. Fluids, 19, 134
Sturrock, P.A. and Uchida, Y., 1981, ApJ, 246, 331
van Ballegoijen, A.A. 1986, ApJ, 311, 1001